

Magnetic resonance imaging reveals neuronal degeneration in the brainstem of the superoxide dismutase 1^{G93A G1H} transgenic mouse model of amyotrophic lateral sclerosis

Da Wei Zang,^{1,2} Qing Yang,¹ Hong Xin Wang,¹ Gary Egan,¹ Elizabeth C Lopes¹ and Surindar S Cheema¹

¹Howard Florey Institute, The University of Melbourne, Parkville, Victoria 3010, Australia

²Department of Anatomy and Cell Biology, Faculty of Medicine, Monash University, Australia

Keywords: hyperintensity, hypointensity, magnetic resonance imaging, motor neuron disease

Abstract

Magnetic resonance imaging (MRI) is becoming the preferred neuroimaging modality for the diagnosis of human amyotrophic lateral sclerosis (ALS). A useful animal model of ALS is the superoxide dismutase 1^{G93A G1H} transgenic mouse, which shows many of the clinico-pathological features of the human condition. We have employed a 4.7-Tesla MRI instrument to determine whether a noninvasive imaging approach can reveal pathological changes in the nervous system of this animal model. Our T₂-weighted MRI revealed consistent changes in brain and brainstem of these mice. Hyperintensities, indicative of neuropathology, were observed in several areas including the nucleus ambiguus, facial nucleus, trigeminal motor nucleus, rostroventrolateral reticular nucleus, lateral paraventricular nucleus and the substantia nigra. Histology analysis including neuronal counts of the imaged brains confirmed the T₂-weighted MRI findings. Enlarged ventricles and hypointense striations, indicative of global atrophy, were also observed in the brain and cerebellum. This atrophy was confirmed by fresh brain weight data. The extensive global degeneration involving multiple structures suggests a multisystem disease that is similar to human ALS.

Introduction

Amyotrophic lateral sclerosis (ALS) is a progressive neuromuscular disorder and the most common form of motor neuron disease (MND). The cause of ALS largely remains unknown and there is no effective treatment to date apart from the modest benefit from Riluzole treatment (Miller, 2003; Miller *et al.*, 2003). The clinical features of human ALS include a combination of upper motor neuron (UMN) and lower motor neuron (LMN) deficits (Cleveland & Rothstein, 2001). LMN symptoms and signs include fatigue, weakness, muscle cramps, atrophy, fasciculations, fibrillations, suppression of reflexes and hypotonia. In contrast, UMN symptoms and signs include incoordination, stiffness, spasticity, hyperreflexia, Babinski reflex and bulbar symptoms.

Magnetic resonance imaging (MRI) as a noninvasive technique is becoming a preferred neuroimaging tool for the diagnosis of ALS. Some specific features in the MRI scans of patients with ALS have been reported; these include low signal intensity and atrophy in cortex using T₁-weighted MRI scanning and increased signal along the corticospinal tract (CST) pathway on T₂-weighted and proton density MRI in the brain and spinal cord (Basak *et al.*, 2002; Sopolana *et al.*, 2002; Hecht *et al.*, 2002; Miwa *et al.*, 2003; Leigh *et al.*, 2002; Ellis *et al.*, 1999). These findings suggest that MRI can detect the

significant degeneration in the central nervous system in ALS patients. In contrast, several other investigations based on MRI (Cheung *et al.*, 1995) or computed tomography (CT; Gallassi *et al.*, 1989) did not reveal significant differences in the incidence of brain atrophy and total brain volumes of grey or white matter (Ellis *et al.*, 2001) between patients with ALS and age-matched controls.

The superoxide dismutase (SOD)1^{G93A G1H} transgenic mouse is a widely used animal model of familial human ALS (Gurney, 1997a; Gurney, 1997b; Ripps *et al.*, 1995; Wong & Borchelt, 1995). In this model, the primary pathology is linked to the degeneration of LMNs in the lumbar spinal cord and brainstem (Lowry *et al.*, 2001). Mice were scored clinically for disease progression as follows: stage I, onset of hindlimb tremor; stage II, onset of hindlimb paresis; stage III, severe hindlimb paresis with abnormal gait; stage IV, hindlimb paralysis; and stage V, death, as described previously (Turner *et al.*, 2003). Significant reductions in the number of dopaminergic nigral (Kostic *et al.*, 1997), corticospinal and bulbospinal (Zang & Cheema, 2002) neurons have also been reported. Quantification of these degenerative changes requires post-mortem tissue and labourious histological preparation and analysis. To date it is not clear whether the additional regions in the brain and brainstem of this mouse model undergo degenerative changes with advanced stages of the disease. An imaging modality based on MRI that is sensitive enough would be ideal to map globally the neurodegenerative changes in animals that die from progressive degenerative disorders such as ALS. To address this issue, we used the 4.7-Tesla MRI instrument in our institute to resolve neuropathological changes in the brain and brainstem of the SOD1^{G93A G1H} transgenic mouse model. In order to validate the

Correspondence: Dr Surindar S. Cheema, Motor Neuron Disease Research Laboratory, Brain Injury and Repair Group, Howard Florey Institute, The University of Melbourne, Victoria 3010, Australia.

E-mail: s.cheema@hfi.unimelb.edu.au

Received 9 May 2004, accepted 28 July 2004

imaging data, we carried out histological assessment of the animals that were used to generate the scans. Our T₂-weighted MRI scans have shown for the first time new structures that undergo pathological changes in this mouse model of ALS.

Materials and methods

Transgenic mice expressing a mutated human SOD1 gene, derived from the B6SJL-TgN (SOD1-G93A) 1 Gur line were purchased from the Jackson Laboratory. These mice were bred and maintained as hemizygotes by mating transgenic males with wild-type (WT) B6SJL females. The Howard Florey Institute Animal Ethics and Experimentation Committee approved all experimental procedures used on mice (Approval number: 03–067).

For MRI imaging, six 120-day-old SOD1^{G93A G1H} transgenic mice and six age-matched WT mice (three males and three females) were investigated with a 4.7-T MR BIOSPEC system (Bruker, Germany) using a microimaging probe. Mice were anaesthetized by continuous inhalation of 1.5–2.5% isoflurane. The respiratory rate was monitored to detect the depth of anaesthesia during the MRI scanning. The anaesthetized animals were mounted in a special mouse holder and the brain and brainstem were scanned. Axial T₂-weighted images were acquired using a RARE (fast spin echo) sequence with repetition time (TR) 5000 ms, echo time (TE) 54 ms, field of view (FOV) 15 × 15 mm with 256 × 256 matrix (in-plane resolution of 58 μm) and slice thickness of 0.5 mm. The scanning time for this high-resolution T₂-weighted imaging was on average 42 min with the number of excitations (NEX) of 16 for 34 slices. The total scanning time including set up was ≈ 1 h. After MRI scanning, the mice were warmed on a heating pad and monitored until they recovered fully.

After MRI scanning, all six SOD1^{G93A G1H} transgenic and six age-matched WT mice were killed with a lethal intraperitoneal injection of 200 mg/kg of sodium pentobarbitone (Rhone Merieux, Australia) and perfused transcardially with 0.1 M mouse-tonicity phosphate-buffered saline (MTPBS), pH 7.4, followed by 4% (w/v) paraformaldehyde. The brain and brainstem were dissected out and postfixed in the same fixative overnight at 4 °C, then transferred to 20% sucrose for 24 h at 4 °C. The brain was mounted into OCT compound (Sakura Finetek, USA) and immediately frozen in isopentane (BDH Laboratory Supplies, UK) which had been cooled on dry ice. The tissues were then sectioned coronally at 30 μm using a cryostat and every fifth section was collected and mounted on superfrost-coated slides. The sections were air-dried, immersed in MTPBS to remove the OCT compound for 20 min and stained in Cresyl Violet for 30 min, rinsed thoroughly in distilled water, differentiated in acid alcohol (three drops of acetic acid to every 100 mL of 95% alcohol) for 5 s, rinsed thoroughly in distilled water, dehydrated and cover-slipped with nonfluorescent DPX plastic mounting media (BOH chemicals; Victoria, Australia). The MRI images and histological sections were then compared with the brain atlas of Paxinos & Franklin (2001) in order to identify the structures that showed hypo- or hyperintensities. The neuronal loss in ambiguous, facial and trigeminal motor nuclei was estimated by counting the number of neurons exhibiting a nucleus within a grid overlay and the data was expressed as mean ± SEM. For tyrosine hydroxylase staining, the brain was sectioned coronally at 10 μm using a cryostat and every fifth section collected and mounted on superfrost-coated slides. The sections were immersed into MTPBS for 5 min to remove the OCT compound. After blocking with 10% horse serum, the sections were incubated with monoclonal mouse antityrosine hydroxylase antibody (catalogue number MAB 5280; Chemicon, CA, USA; diluted 1 : 500) overnight at 4 °C, and followed by biotinylated secondary antibodies (horse antimouse 1 : 100;

Sigma-Aldrich Pty Ltd, Sydney, Australia) and fluorescein avidin (Vector laboratory, Inc., Burlingame, USA), and then cover-slipped using fluorescent mounting media (DAKO, CA, USA). The images of tyrosine hydroxylase-positive neurons were captured ×40 using Microfire software (Olympus, USA).

To confirm the atrophy in mouse brain, six age-matched SOD1^{G93A G1H} transgenic and six WT mice (three males and three females) were killed by a lethal intraperitoneal injection of 200 mg/kg of sodium pentobarbitone and the brain and brainstem were dissected out and detached from the spinal cord at the level of the first cervical vertebra (C1). The fresh brain and brainstem were weighed together and the data was expressed as mean ± SEM.

Results

In the six transgenic and six age- and gender-matched WT mice, T₂-weighted MRI coronal images were obtained from the frontal cortex through to the brainstem medulla. In some animals coronal images were obtained from the cervical and upper thoracic cords. Hyperintense areas that reflect regions of neurodegeneration were found primarily in the brainstem. Strong hyperintense regions were found primarily in the following three cranial nerve nuclei: nucleus ambiguus, facial nucleus and motor trigeminal nucleus. It should be noted that hypointense areas indicative of diffuse atrophy were also detected in the brain and cerebellum in the transgenic mice.

The nucleus ambiguus in the SOD1^{G93A G1H} transgenic mice showed prominent hyperintensities bilaterally in T₂-weighted MRI images (Fig. 1A, arrows). Such a signal was not detected in the age- and gender-matched WT mice (Fig. 1B). After completion of the MRI, the brains and spinal cords were cut and stained with Cresyl Violet. In these histological sections, the imaged hyperintense regions corresponded to the nucleus ambiguus (Fig. 1C, arrows) and this was confirmed using the mouse brain atlas (Fig. 1D, arrows). At higher magnification (Fig. 1E) the nucleus ambiguus in the transgenic mice shows intense vacuolation and neuronal loss compared to the WT control mouse (Fig. 1F). This loss was bilateral and can be seen in Fig. 1C. The histogram in Fig. 1G summarizes the number of neurons in the nucleus ambiguus of 120-day-old SOD1^{G93A G1H} transgenic and WT mice. In the SOD1^{G93A G1H} transgenic mice a total 49 ± 8 neurons were counted compared to 124 ± 13 in the WT controls. This represents a reduction of 60% ($P < 0.001$) in SOD1^{G93A G1H} transgenic mice. It should also be noted that hyperintensities were also associated with the rostroventrolateral reticular nucleus and the lateral paragigantocellular nucleus (Fig. 1A, arrowheads). However, in the corresponding histological sections the degeneration was not obvious in these areas of the brainstem.

The facial nucleus had prominent hyperintensities bilaterally in T₂-weighted MRI images in the SOD1^{G93A G1H} transgenic mice compared to WT mice (arrows in Fig. 1H and I), respectively. Sections from the mouse brain atlas indicate that the imaged hyperintense areas correspond to the facial nucleus (Fig. 1J and K, arrows). The facial nucleus in the transgenic mice shows intense vacuolation and neuronal loss compared to the WT control mouse (Fig. 1L and M). The histogram in Fig. 1N summarizes the number of the neurons in the facial nucleus of 120-day-old SOD1^{G93A G1H} transgenic and WT mice. In the SOD1^{G93A G1H} transgenic mice a total 244 ± 46 neurons were counted compared to 485 ± 48 in the WT controls. This represents a reduction of 50% ($P < 0.005$) in SOD1^{G93A G1H} transgenic mice.

Hyperintense signals were detected bilaterally in the trigeminal motor nucleus of the SOD1^{G93A G1H} transgenic mice (Fig. 2A, arrows). Such hyperintensity was not detected in WT mice (Fig. 2B). Correlations with Cresyl Violet-stained sections of the imaged brains

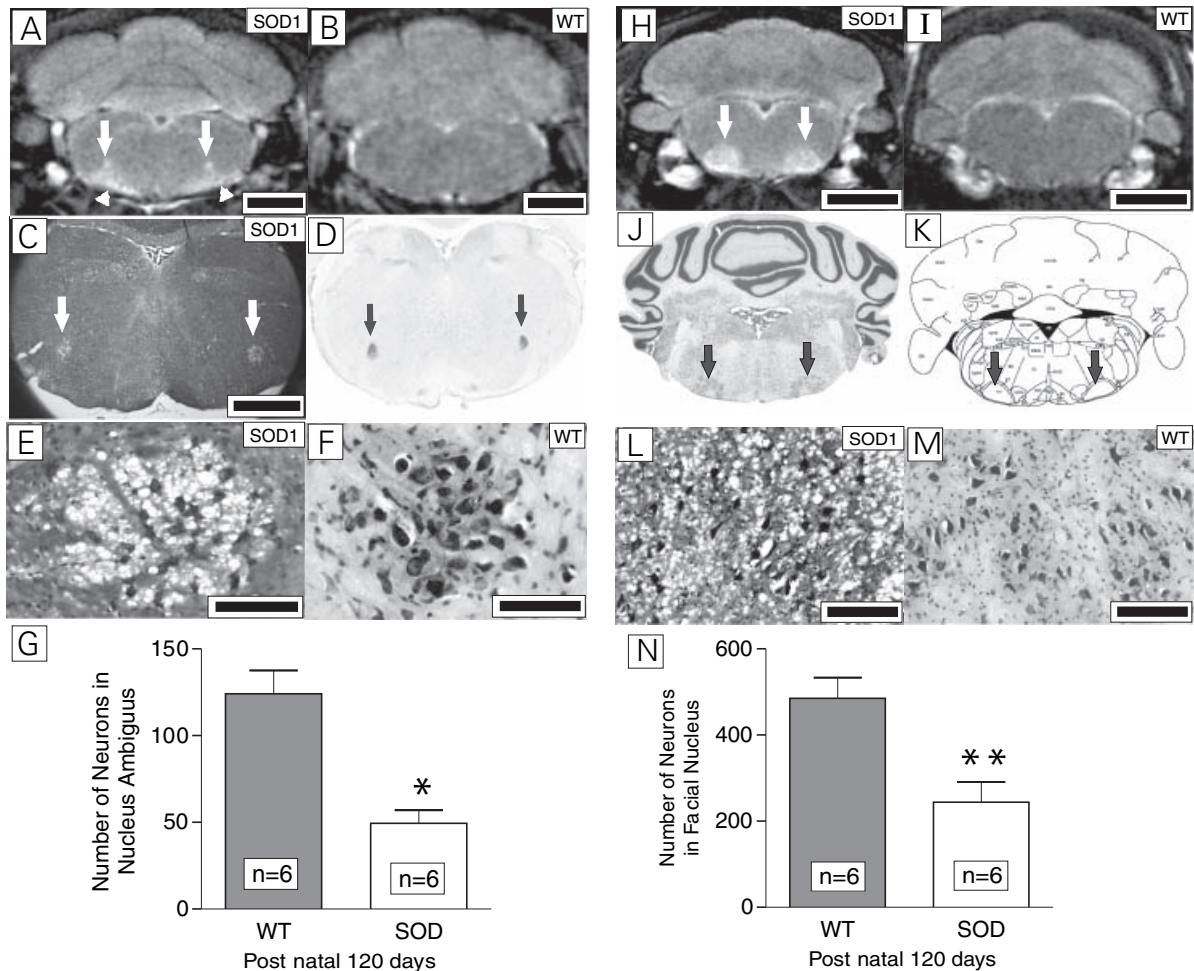


FIG. 1. T₂-weighted MRI and histology showing neurodegenerative changes in the brainstem and the facial nucleus of a 120-day-old WT and SOD1^{G93A G1H} transgenic mouse. The T₂-weighted MRI hyperintense regions are detectable in several brainstem areas of the SOD1^{G93A G1H} transgenic mouse including (A, arrows) the nucleus ambiguus, (A, arrowheads) the rostroventrolateral reticular nucleus and the lateral paragigantocellular nucleus compared to (B) the WT mouse. (C and E) Nissl-stained sections obtained from the SOD1^{G93A G1H} transgenic mouse illustrated in panel A. (D) Also included is a reference section of the corresponding level from the mouse brain atlas of Paxinos & Franklin (2001). These sections demonstrate that the prominent hyperintensity in the noninvasive images can be linked to the vacuolar degeneration in nucleus ambiguus. (F) Normal histological appearance of the nucleus ambiguus in a WT mouse compared to the extensive vacuolar degeneration in (E) the transgenic mouse. (G) The histogram shows a statistically significant reduction in the number of neurons in nucleus ambiguus of the SOD1^{G93A G1H} transgenic mice. (H and I, arrows) The T₂-weighted MRI hyperintensity is located in the facial nucleus of the SOD1^{G93A G1H} transgenic mouse compared to the WT mouse. (J,K, arrows) Reference sections of the matching levels from the mouse brain atlas of Paxinos & Franklin (2001) show the hyperintense areas correspond to the facial nucleus. (L) Photomicrograph showing intense vacuolar degeneration in the facial nucleus in a Nissl-stained section obtained from the SOD1^{G93A G1H} transgenic mouse which was used to obtain image H. (M) Normal histological appearance of the facial nucleus from an age- and gender-matched WT mouse. (N) The histogram shows a statistically significant reduction in the number of neurons in the facial nucleus of SOD1^{G93A G1H} transgenic mice; **P* < 0.001, ***P* < 0.005. Scale bars, 2 mm (A, B, H and I), 200 μm (C), 20 μm (E and F), 50 μm (L and M).

and the mouse brain atlas indicate that the imaged hyperintense areas correspond to the trigeminal motor nucleus (Fig. 2C and D, arrows). The trigeminal motor nucleus in the transgenic mice contained intense vacuolation and had prominent neuronal loss compared to the WT control mouse (Fig. 2E and F). The histogram in Fig. 2G summarizes the neuronal numbers in the trigeminal motor nucleus of 120-day-old SOD1^{G93A G1H} transgenic and WT mice. In the SOD1^{G93A G1H} transgenic mice a total 128 ± 10 neurons were counted compared to 225 ± 19 in the WT controls. This represents a reduction of 43% (*P* < 0.005) in SOD1^{G93A G1H} transgenic mice.

The substantia nigra also showed hyperintensities bilaterally in T₂-weighted MRI images in SOD1^{G93A G1H} transgenic mice but not in WT mice (Fig. 2H and I, arrows). Higher magnifications of the hyperintense regions are shown in Fig. 2J and K. Histological sections of the imaged brains and reference to the mouse brain atlas indicate

that the imaged hyperintense areas correspond to the substantia nigra (Fig. 2L and M, arrows). There is a clear reduction in the number of neurons in substantia nigra in SOD1^{G93A G1H} transgenic mice (Fig. 2N) compared to WT mice (Fig. 2O). Immunostaining also confirmed the loss of tyrosine hydroxylase neurons in pars compacta of the substantia nigra in SOD1^{G93A G1H} transgenic mice (Fig. 2P) compared with WT mice (Fig. 2Q).

T₂-weighted MRI also detected an enlarged lateral recess of the 4th ventricle (arrows) and aqueduct (Fig. 3A arrows and Fig. 3E arrowhead) in SOD1^{G93A G1H} transgenic mice but not in WT mice (Fig. 3B and F). Hypointensity striations in the cerebellum were detected in the SOD1^{G93A G1H} transgenic mice (Fig. 3C, arrows) but these were absent in the WT mice (Fig. 3D). Hypointensity striations between the midbrain and cerebral cortex were detected on T₂-weighted MRI but not detectable in the WT mice (Fig. 3E and

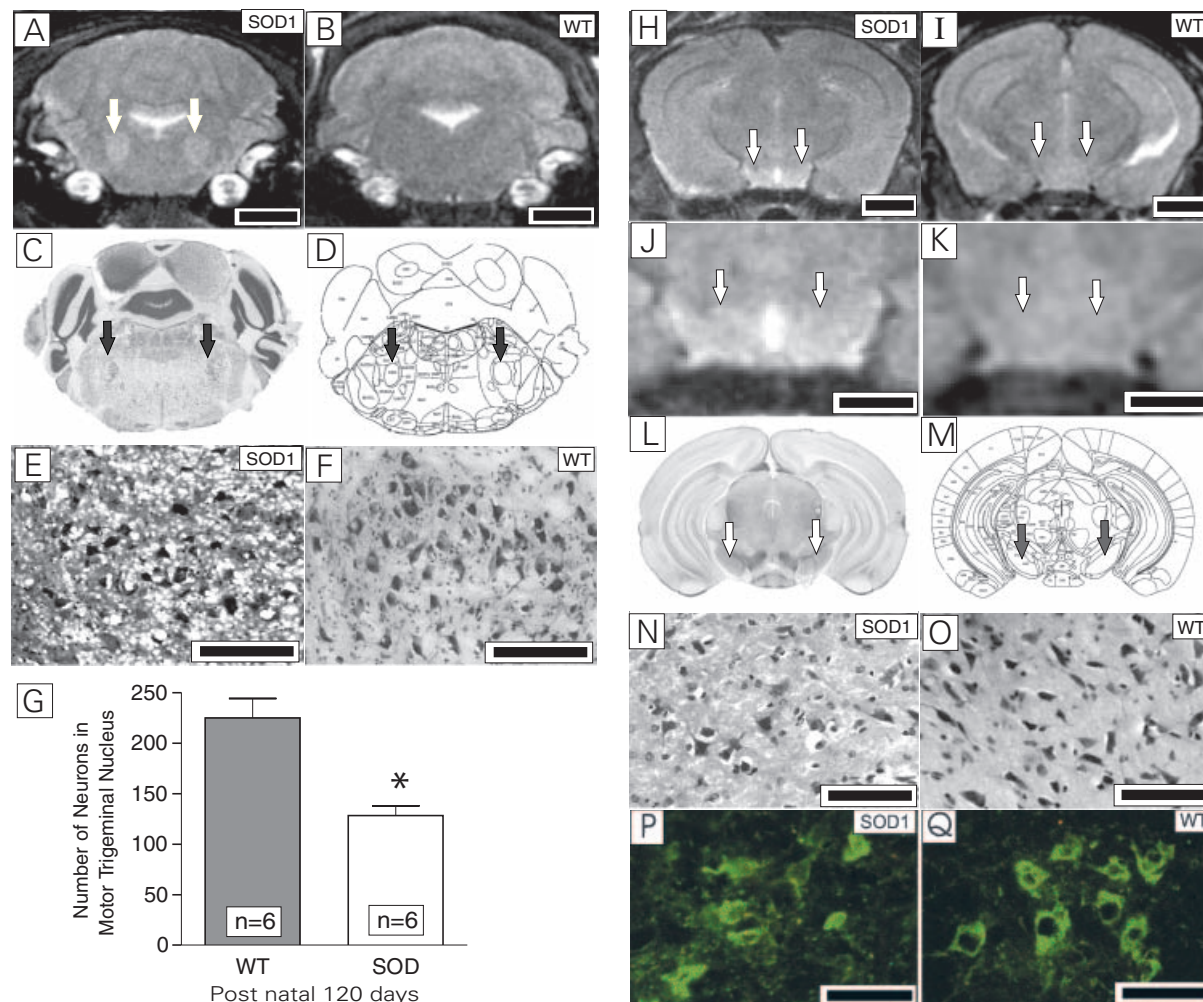


FIG. 2. T₂-weighted MRI images and histology showing neurodegenerative changes in the motor trigeminal nucleus and the substantia nigra of a 120-day-old WT and SOD1^{G93A G1H} transgenic mouse. (A, arrows) The T₂-weighted MRI hyperintensity in the SOD1^{G93A G1H} transgenic mouse corresponds to the motor trigeminal nucleus. (B) Note the absence of a similar hyperintensity in the WT mouse. (C, D, arrows) Reference sections of the matching levels from the mouse brain atlas of Paxinos & Franklin (2001) show the hyperintense areas correspond to the trigeminal motor nucleus. (E) Photomicrograph showing intense vacuolar degeneration in the motor trigeminal nucleus in a Nissl-stained section obtained from the SOD1^{G93A G1H} transgenic mouse which was used to obtain image A. (F) Normal histological appearance of the motor trigeminal nucleus from a age- and gender-matched WT mouse. (G) The histogram shows a statistically significant reduction in the number of neurons in trigeminal motor nucleus of SOD1^{G93A G1H} transgenic mice. (H, arrows) The T₂-weighted MRI hyperintensity in the SOD1^{G93A G1H} transgenic mouse corresponds to the midbrain substantia nigra. (I, arrows) Note the absence of a similar hyperintensity in the WT mouse. (J and K, arrows) These changes are also illustrated at higher magnifications. (L, M, arrows) Reference sections of the matching levels from the mouse brain atlas of Paxinos & Franklin (2001) show the hyperintense areas correspond to the substantia nigra. (N) Photomicrograph showing vacuolar degeneration in the substantia nigra in a Nissl-stained section obtained from the SOD1^{G93A G1H} transgenic mouse which was used to obtain image H. (O) Normal histological appearance of the substantia nigra from a WT mouse. (P, Q) Photomicrographs showing a decrease in the number of tyrosine hydroxylase-positive neurons in the substantia nigra of the SOD1^{G93A G1H} transgenic (P) mouse compared to the WT (Q) control. **P* < 0.001. Scale bars, 2 mm (A, B, H and I), 20 μm (E, F, N and O), 1 mm (J and K) and 50 μm (P and Q).

F). These hypointensity striations were also found in the lateral cerebral cortex of SOD1^{G93A G1H} transgenic mice (Fig. 3G, arrows) but were absent in the WT mice (Fig. 3H). The histogram in Fig. 3I shows the brain weight loss in SOD1^{G93A G1H} transgenic mice at 120 postnatal days. A brain weight loss of 11% (*P* < 0.05) was detected in SOD1 mice (0.4141 ± 0.0077 g) compared to WT mice (0.4634 ± 0.0059 g).

Discussion

Amyotrophic lateral sclerosis in humans is often characterized by the degeneration of lower and upper motor neurons. Despite the loss of corticospinal neurons in the SOD1^{G93A G1H} transgenic mouse, it is difficult to evaluate UMN disease signs (Zang & Cheema, 2002). To

date, all experiments involving assessment of UMN degeneration in such mouse model of ALS required that the animal be killed in order to assess the degeneration in the central nervous system. The aim of this study was to develop a noninvasive modality to visualize the degeneration in the central nervous system of this mouse model of ALS. For this study, we chose MRI because it is a powerful imaging tool that has been used to reveal neuropathologic changes in the human brain and spinal cord of patients with ALS (Basak *et al.*, 2002; Ellis *et al.*, 1999; Ellis *et al.*, 2001). Such a noninvasive approach could be especially useful for tracking neurodegenerative changes in the living mouse undergoing experimental drug therapy. It has been reported that MRI can reveal subtle atrophy in the human brain that is difficult to visualize in post-mortem tissue (Ellis *et al.*, 2001).

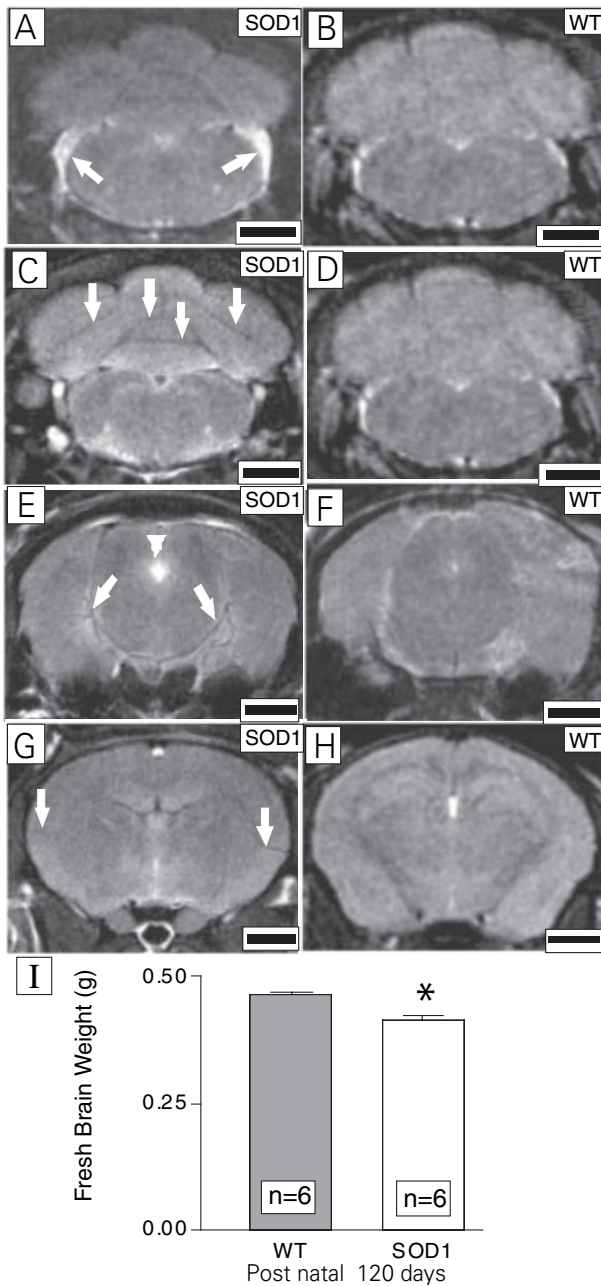


FIG. 3. T2-weighted MRI showing atrophy in the brain and cerebellum of SOD1^{G93A G1H} transgenic mice. (A, B, E and F) T2-weighted MRI hyperintense areas were detected in several regions including the enlarged lateral recess of the 4th ventricle (A, arrows) and cerebral aqueduct (E, arrowhead) compared to age- and gender-matched WT mice (B and F). (C, E and G) It should be noted that hypointense striations were also detected on T₂ imaging in cerebellum (C, arrows), the lateral spaces between brain and midbrain (E, arrows) and in the lateral part of the forebrain corresponding to the lateral fissure (G, arrows). These changes were only detected in SOD1^{G93A G1H} transgenic mice but not in (D, F and H) the WT mice. (I) Histogram showing a statistically significant reduction in the brain weight of the SOD1^{G93A G1H} transgenic mice compared to the WT animals. **P* < 0.05. Scale bars, 2 mm.

This report shows for the first time that T2-weighted MRI reveals neurodegenerative and atrophic pathology in the brain of living SOD1^{G93A G1H} transgenic mice. It is generally accepted that neurodegenerative disease is associated with hyperintense signals on T₂ and hypointense signals on T₁ (Table 1). Neurodegenerative changes

TABLE 1. Interpretation of hyper- and hypo-intensity signals in T2-weighted MRI of the mouse in this study

Signal	Pathology	Water level
Hyperintensity	Vacuolation	High
Hypointensity	Atrophy not detectable <i>post-mortem</i>	Low

reflected by clear T2-weighted MRI hyperintensity were detected in several nuclei including the ambiguus, facial, motor trigeminal and lateral paraventricular, and the rostroventrolateral reticular area and the substantia nigra. Furthermore, atrophic changes reflected by T2-weighted MRI hypointensity striations in the cerebral cortex, cerebellum and brainstem, as well as enlarged ventricles, were detected.

The pathology revealed by our T2-weighted MRI imaging corresponding to nucleus ambiguus, facial and motor trigeminal nucleus in SOD1^{G93A G1H} transgenic mice are supported by published reports in other mouse models of ALS. Nimchinsky *et al.* (2000) showed, using histological methods in the SOD1G86R transgenic mouse, that the facial but not the oculomotor or hypoglossal nuclei undergo degeneration. They reported a 48% neuronal loss in the facial nucleus; our study showed a 50% loss. Our study and those of others indicate the sparing of the oculomotor and trochlear nuclei in these mouse models of ALS (Haenggeli & Kato, 2002). Furthermore, our study reveals that the hypoglossal nucleus is also spared. Most importantly, our T2-weighted MRI imaging points to a severe pathology in the nucleus ambiguus and motor trigeminal nucleus. These findings predict that at disease end-stage, these mice have deficits in the movement of the larynx and pharynx attributable to the degeneration in nucleus ambiguus, deficits of facial expression due to degeneration of the facial nucleus and reduced mastication due to the pathology associated with the degeneration in the motor trigeminal nucleus. Thus MRI is a sensitive, noninvasive approach for detecting underlying pathology during the end stages of the disease. Furthermore, this study predicts for the first time that the SOD1^{G93A G1H} transgenic mice have deficits in vocalization, mastication and swallowing. These functions are not easily measured by clinical examination and require further analysis. The deficits in mastication and swallowing could exacerbate the weight loss that is usually attributed to muscular atrophy. Human patients with bulbar onset ALS typically have progressive loss of speech and ability to masticate and to swallow food. The MRI findings in this study reveal close correlations in the pathology between the SOD1^{G93A G1H} transgenic mouse brainstem and human patients with bulbar onset ALS.

It should be noted that, in this study, the MRI images correlated highly with the post-mortem histology of the same brains. In the nucleus ambiguus, facial and motor trigeminal nuclei extensive loss of motor neurons and vacuolation could be seen in Cresyl Violet-stained sections. Neuronal counts revealed losses of 60, 50 and 43%, respectively. Hyperintensities were also found bilaterally in substantia nigra of the brain in SOD1^{G93A G1H} transgenic mice, and a clear reduction in neuronal number was observed in the histological sections. The loss of dopaminergic neurons in substantia nigra revealed by the MRI images is consistent with previous reports (Kostic *et al.*, 1997). Thus in these mice the degeneration of the nigrostriatal system is likely to compound the ALS syndrome. Our results suggest that at the end stage of the disease these mice may have deficits such as bradykinesia which are attributable to the degeneration of the nigrostriatal pathway on top of the progressive paralysis due to primary motor neuron loss in the brainstem and spinal cord. It should

be noted that there is a form of human ALS that is associated with Parkinsonian symptoms (Kokubo & Kuzuhara, 2003; Zoccollella *et al.*, 2002). These findings support the view that the SOD1^{G93A G1H} transgenic mouse of ALS is a multi-system syndrome.

In our study, we consistently found hypointensity striations in the cerebellum and cerebral cortex in the SOD1^{G93A G1H} transgenic mice. This suggests that T2-weighted MRI imaging is also a reliable noninvasive tool for the detection of brain atrophy in the mice. A significant loss of brain weight was also confirmed. The nature and mechanism for the formation of the hypointensity striations in the SOD1^{G93A G1H} transgenic mice is not clear because a corresponding pathology cannot be detected in the post-mortem brains. It is possible that in the lissencephalic mouse cortex these striations represent planes in the brain and cerebellum where there is less water due to the atrophy. Enlargement of the lateral recess of the 4th ventricle was also detected in two of six SOD1^{G93A G1H} transgenic mice, but in none of the WT mice. These findings suggest that, in the diseased mice, the atrophy of the brainstem is variable and this requires further investigation into the differential atrophy involving specific structures including sensorimotor cortex, internal capsule and brainstem.

Our findings indicate that T2-weighted MRI scanning is a reliable imaging modality for detecting the degeneration and atrophy in the brain of SOD1^{G93A G1H} transgenic mice. Hyperintensities in proton-density-weighted MR (Cheung *et al.*, 1995) and T₂-weighted MRI images in white matter along the CST have been reported in human ALS (Hecht *et al.*, 2002; Peretti-Viton *et al.*, 1999; Hofmann *et al.*, 1998; Yagishita, 1995); however, any pathology in the mouse CST was beyond the resolving power of our T2-weighted MRI scans. Some changes in the CST should be anticipated because loss of corticospinal neurons has been recently reported from our laboratory (Zang & Cheema, 2002). Furthermore, we did not observe abnormal signals associated with the white matter of SOD1^{G93A G1H} transgenic mice; it is possible that our imaging protocol may not be sensitive enough to resolve subtle degeneration in white matter of SOD1^{G93A G1H} transgenic mice. Other imaging methods including quantitative T2 mapping (Usov *et al.*, 1999; Pfund *et al.*, 2003; Konagaya *et al.*, 2002), diffusion-weighted imaging (Horsfield & Jones, 2002), diffusion-tensor imaging (Sach *et al.*, 2003; Gossel *et al.*, 2002; Toosy *et al.*, 2003) or MR spectroscopy (Kalra *et al.*, 2003; Kaufmann & Mitsumoto, 2002; Suhy *et al.*, 2002; Sarchielli *et al.*, 2001) may further enhance the power of MRI as a noninvasive method for tracking disease pathology in both grey and white matter in the SOD1^{G93A G1H} transgenic mouse model of ALS. The findings reported in this paper should provide an impetus for the further noninvasive tracking of disease progression and neuropathology in response to novel drug therapies in this mouse model.

Acknowledgements

We thank the following organizations for their financial support: The Motor Neuron Disease Research Institute of Australia, The Amyotrophic Lateral Sclerosis Association of the United States, The National Health and Medical Research Council of Australia (NHMRC Program Grant: 236805) and NHMRC Transitional Institute Grant (Program Grant: 217299). We also thank Dr Alvin Quah and Mr Bradley Turner for useful comments on the manuscript.

Abbreviations

ALS, amyotrophic lateral sclerosis; CST, corticospinal tract; CT, computed tomography; LMN, lower motor neuron; MND, motor neuron disease; MRI, magnetic resonance imaging; SOD, superoxide dismutase; UMN, upper motor neuron; WT, wild-type.

References

- Basak, M., Erturk, M., Oflazoglu, B., Ozel, A., Yildiz, G.B. & Forta, H. (2002) Magnetic resonance imaging in amyotrophic lateral sclerosis. *Acta Neurol. Scand.*, **105**, 395–399.
- Cheung, G., Gawel, M.J., Cooper, P.W., Farb, R.I., Ang, L.C. & Gawal, M.J. (1995) Amyotrophic lateral sclerosis: correlation of clinical and MR imaging findings. *Radiology*, **194**, 263–270.
- Cleveland, D.W. & Rothstein, J.D. (2001) From Charcot to Lou Gehrig: deciphering selective motor neuron death in ALS. *Nat. Rev. Neurosci.*, **2**, 806–819.
- Ellis, C.M., Simmons, A., Dawson, J.M., Williams, S.C. & Leigh, P.N. (1999) Distinct hyperintense MRI signal changes in the corticospinal tracts of a patient with motor neuron disease. *Amyotroph Lateral Scler Other Motor Neuron Disord*, **1**, 41–44.
- Ellis, C.M., Suckling, J., Amaro, E. Jr, Bullmore, E.T., Simmons, A., Williams, S.C. & Leigh, P.N. (2001) Volumetric analysis reveals corticospinal tract degeneration and extramotor involvement in ALS. *Neurology*, **57**, 1571–1578.
- Gallassi, R., Montagna, P., Morreale, A., Lorusso, S., Tinuper, P., Daidone, R. & Lugaresi, E. (1989) Neuropsychological, electroencephalogram and brain computed tomography findings in motor neuron disease. *Eur. Neurol.*, **29**, 115–120.
- Gossel, C., Fahrmeier, L., Putz, B., Auer, L.M. & Auer, D.P. (2002) Fiber tracking from DTI using linear state space models: detectability of the pyramidal tract. *Neuroimage*, **16**, 378–388.
- Gurney, M.E. (1997a) Transgenic animal models of familial amyotrophic lateral sclerosis. *J. Neurol.*, **244**, S15–S20.
- Gurney, M.E. (1997b) The use of transgenic mouse models of amyotrophic lateral sclerosis in preclinical drug studies. *J. Neurol. Sci.*, **152**, S67–S73.
- Haenggeli, C. & Kato, A.C. (2002) Differential vulnerability of cranial motoneurons in mouse models with motor neuron degeneration. *Neurosci. Lett.*, **335**, 39–43.
- Hecht, M.J., Fellner, F., Fellner, C., Hilz, M.J., Neundorfer, B. & Heuss, D. (2002) Hyperintense and hypointense MRI signals of the precentral gyrus and corticospinal tract in ALS: a follow-up examination including FLAIR images. *J. Neurol. Sci.*, **199**, 59–65.
- Hofmann, E., Ochs, G., Pelzl, A. & Warmuth-Metz, M. (1998) The corticospinal tract in amyotrophic lateral sclerosis: an MRI study. *Neuroradiology*, **40**, 71–75.
- Horsfield, M.A. & Jones, D.K. (2002) Applications of diffusion-weighted and diffusion tensor MRI to white matter diseases – a review. *NMR Biomed*, **15**, 570–577.
- Kalra, S., Cashman, N.R., Caramanos, Z., Genge, A. & Arnold, D.L. (2003) Gabapentin therapy for amyotrophic lateral sclerosis: lack of improvement in neuronal integrity shown by MR spectroscopy. *Am. J. Neuroradiol.*, **24**, 476–480.
- Kaufmann, P. & Mitsumoto, H. (2002) Amyotrophic lateral sclerosis: objective upper motor neuron markers. *Curr. Neurol. Neurosci. Rep.*, **2**, 55–60.
- Kokubo, Y. & Kuzuhara, S. (2003) Neuroradiological study of patients with amyotrophic lateral sclerosis and parkinsonism–dementia complex on the Kii peninsula of Japan. *Arch. Neurol.*, **60**, 1257–1261.
- Konagaya, M., Matsuoka, Y. & Konagaya, Y. (2002) [Quantitative MRI study of progressive cerebral atrophy in multiple system atrophy]. *Rinsho Shinkeigaku*, **42**, 118–125.
- Kostic, V., Gurney, M.E., Deng, H.X., Siddique, T., Epstein, C.J. & Przedborski, S. (1997) Midbrain dopaminergic neuronal degeneration in a transgenic mouse model of familial amyotrophic lateral sclerosis. *Ann. Neurol.*, **41**, 497–504.
- Leigh, P.N., Simmons, A., Williams, S., Williams, V., Turner, M. & Brooks, D. (2002) Imaging: MRS/MRI/PET/SPECT: summary. *Amyotroph Lateral Scler Other Motor Neuron Disord*, **3**, S75–S80.
- Lowry, K.S., Murray, S.S., McLean, C.A., Talman, P., Mathers, S., Lopes, E.C. & Cheema, S.S. (2001) A potential role for the p75 low-affinity neurotrophin receptor in spinal motor neuron degeneration in murine and human amyotrophic lateral sclerosis. *Amyotroph Lateral Scler Other Motor Neuron Disord*, **2**, 127–134.
- Miller, R. (2003) Riluzole for ALS: what is the evidence. *Amyotroph Lateral Scler Other Motor Neuron Disord*, **4**, 135.
- Miller, R.G., Mitchell, J.D., Lyon, M. & Moore, D.H. (2003) Riluzole for amyotrophic lateral sclerosis (ALS) /motor neuron disease (MND). *Amyotroph Lateral Scler Other Motor Neuron Disord*, **4**, 191–206.
- Miwa, H., Kajimoto, Y., Nakanishi, I., Morita, S., Komoto, J., Kihira, T. & Kondo, T. (2003) T2-low signal intensity in the cortex in multiple system atrophy. *J. Neurol. Sci.*, **211**, 85–88.
- Nimchinsky, E.A., Young, W.G., Yeung, G., Shah, R.A., Gordon, J.W., Bloom, F.E., Morrison, J.H. & Hof, P.R. (2000) Differential vulnerability of

- oculomotor, facial, and hypoglossal nuclei in G86R superoxide dismutase transgenic mice. *J. Comp. Neurol.*, **416**, 112–125.
- Paxinos, G. & Franklin, K. (2001) *The Mouse Brain in Stereotaxic Coordinates*. Academic Press, Sydney, Australia.
- Peretti-Viton, P., Azulay, J.P., Trefouret, S., Brunel, H., Daniel, C., Viton, J.M., Flori, A., Salazard, B., Pouget, J., Serratrice, G. & Salamon, G. (1999) MRI of the intracranial corticospinal tracts in amyotrophic and primary lateral sclerosis. *Neuroradiology*, **41**, 744–749.
- Pfund, Z., Kagawa, K., Juhasz, C., Shen, C., Lee, J.S., Chugani, D.C., Muzik, O. & Chugani, H.T. (2003) Quantitative analysis of gray- and white-matter volumes and glucose metabolism in Sturge–Weber syndrome. *J. Child Neurol.*, **18**, 119–126.
- Ripps, M.E., Huntley, G.W., Hof, P.R., Morrison, J.H. & Gordon, J.W. (1995) Transgenic mice expressing an altered murine superoxide dismutase gene provide an animal model of amyotrophic lateral sclerosis. *Proc. Natl Acad. Sci. USA*, **92**, 689–693.
- Sach, M., Winkler, G., Glauche, V., Liepert, J., Heimbach, B., Koch, M.A., Buchel, C. & Weiller, C. (2003) Diffusion tensor MRI of early upper motor neuron involvement in amyotrophic lateral sclerosis. *Brain*, **127**, 340–350.
- Sarchielli, P., Pelliccioli, G.P., Tarducci, R., Chiarini, P., Presciutti, O., Gobbi, G. & Gallai, V. (2001) Magnetic resonance imaging and 1H-magnetic resonance spectroscopy in amyotrophic lateral sclerosis. *Neuroradiology*, **43**, 189–197.
- Sopelana, D., Vazquez, A.V., Marcos, A., Arroyo, R. & Varela De Seijas, E. (2002) [Wallerian degeneration of the pyramidal bundle and amyotrophic lateral sclerosis in MRI]. *Neurologia*, **17**, 218.
- Suhy, J., Miller, R.G., Rule, R., Schuff, N., Licht, J., Dronsky, V., Gelinas, D., Maudsley, A.A. & Weiner, M.W. (2002) Early detection and longitudinal changes in amyotrophic lateral sclerosis by (1) H MRSI. *Neurology*, **58**, 773–779.
- Toosy, A.T., Werring, D.J., Orrell, R.W., Howard, R.S., King, M.D., Barker, G.J., Miller, D.H. & Thompson, A.J. (2003) Diffusion tensor imaging detects corticospinal tract involvement at multiple levels in amyotrophic lateral sclerosis. *J. Neurol. Neurosurg Psychiatry*, **74**, 1250–1257.
- Turner, B.J., Cheah, I.K., Macfarlane, K.J., Lopes, E.C., Petratos, S., Langford, S.J. & Cheema, S.S. (2003) Antisense peptide nucleic acid-mediated knockdown of the p75 neurotrophin receptor delays motor neuron disease in mutant SOD1 transgenic mice. *J. Neurochem.*, **87**, 752–763.
- Usov, V., Iaroshevskii, S.P., Sinityn, V.E., Plotnikov, M.P. & Zavadovskaia, V.D. (1999) [Quantification of volume of tissue damage in stroke using T2-weighted MRI images]. *Vestn. Rentgenol. Radiol.*, **2**, 9–13.
- Wong, P.C. & Borchelt, D.R. (1995) Motor neuron disease caused by mutations in superoxide dismutase 1. *Curr. Opin. Neurol.*, **8**, 294–301.
- Yagishita, A. (1995) [MR imaging of the brain of amyotrophic lateral sclerosis]. *Rinsho Shinkeigaku*, **35**, 1554–1556.
- Zang, D.W. & Cheema, S.S. (2002) Degeneration of corticospinal and bulbospinal systems in the superoxide dismutase 1 (G93A G1H) transgenic mouse model of familial amyotrophic lateral sclerosis. *Neurosci. Lett.*, **332**, 99–102.
- Zoccolella, S., Palagano, G., Fraddosio, A., Russo, I., Ferrannini, E., Serlenga, L., Maggio, F., Lamberti, S. & Iliceto, G. (2002) ALS-plus: 5 cases of concomitant amyotrophic lateral sclerosis and parkinsonism. *Neurol. Sci.*, **23**, S123–S124.